



# Effect of urbanization on surface runoff and performance of green roofs and permeable pavement for mitigating urban floods

Şevki Öztürk<sup>1</sup> · Kutay Yılmaz<sup>2</sup> · A. Ersin Dinçer<sup>3</sup> · Volkan Kalpakçı<sup>4</sup>

Received: 4 October 2023 / Accepted: 12 May 2024 / Published online: 29 May 2024  
© The Author(s) 2024

## Abstract

Floods are increasingly becoming a significant concern due to climate change, global warming, and excessive urbanization. The Intergovernmental Panel on Climate Change (IPCC) has projected that global warming will continue to contribute to more frequent and severe floods and hydrological extremes. In response to these challenges, nature-based solutions (NBSs) have gained recognition as effective approaches to mitigate the adverse impacts of floods by focusing on ecosystem conservation, restoration, and sustainable utilization of natural resources. This study examines a flood that occurred in the Erkilet District of Kayseri, Türkiye on September 22, 2022, as a result of intense rainfall. It involves a thorough on-site investigation to assess the hydraulic, hydrologic, and geotechnical attributes of the study area. The findings from the field study indicate that the primary cause of the flood is attributed to excessive urbanization. To further analyze the impact of urbanization, a hydraulic model is developed considering both the physical and topographical conditions of the study area for both the year 2006 and 2022. The simulation results reveal that the extent of inundation area and water depth has increased significantly due to the excessive urbanization that occurred within a 16-year period. Additionally, the effectiveness of green roofs and permeable pavements as NBSs to mitigate urban flooding is explored. The implementation of green roofs and permeable pavements shows promising results, reducing the adverse effects of urban floods by 3% to 8%, depending on their specific locations and configurations. However, the results suggest that NBSs alone cannot fully prevent floods so they should complement gray infrastructure. The novelty of the study lies in its ability to demonstrate the impact of urbanization and the effectiveness of nature-based solutions in mitigating flood extent based.

**Keywords** Floods · Nature based solution · Soil gradation · Infiltration · Excess precipitation · Hydraulic modeling · Green roofs · Permeable pavements

---

✉ A. Ersin Dinçer  
ersin.dincer@agu.edu.tr

<sup>1</sup> Department of Civil Engineering, Geotechnics Division, Çankaya University, Ankara, Turkey

<sup>2</sup> Department of Civil Engineering, Hydraulics Division, Yaşar University, İzmir, Turkey

<sup>3</sup> Department of Civil Engineering, Hydraulics Division, Abdullah Gül University, Kayseri, Turkey

<sup>4</sup> Department of Civil Engineering, Middle East Technical University, Ankara, Turkey

## 1 Introduction

Floods are frequent and destructive natural hazards that can result in the loss of lives, livestock, and economic assets on a global scale (Slater and Villarini 2016; Alfieri et al. 2017; Kreibich et al. 2017; Zhai et al. 2020). Studies have shown that while floods are a natural phenomenon, excess urbanization and climate change have an increasing impact on their recurrence and extent (Alfieri et al. 2017; Du et al. 2019). Furthermore, the Intergovernmental Panel on Climate Change (IPCC) reported that future projections under various climate change scenarios suggest an increase in river flooding and extreme runoff and flows (Alfieri et al. 2017; Kreibich et al. 2017; Zhai et al. 2020; Slater et al. 2021; Yılmaz et al. 2022, 2023b; IPCC 2022).

To further understand the impacts of climate change on floods, Alfieri et al. (2017) conducted a global assessment of the frequency and magnitude of river floods under global temperature increase scenarios of 1.5 °C, 2 °C, and 4 °C. The study found an increasing trend in annual precipitation maxima for the entire land surface. Moreover, it is found that flood events with occurrence intervals larger than the return period of present flood protections are projected to rise on all continents under all scenarios leading to a widespread increase in the flood hazard.

In a similar study, Döll et al. (2018) projected a significant increase in high flows in the event of a global temperature increase of 1.5 °C and 2.0 °C. Furthermore, the IPCC's report (2022) highlights a high likelihood that global warming of 2.0 °C above pre-industrial levels will lead to an expansion of flood-prone areas and substantial increases in runoff. The report provides a summarized global warming scenario, with a medium level of confidence in this projection.

In addition to the negative effects of climate change, excessive and incorrect urbanization can increase the effects of natural hazards, particularly floods. Urbanization typically involves a rapid reduction in pervious areas, leading to urban flooding. The process of urbanization typically involves a consistent increase in impervious surfaces (Ercolani et al. 2018). Urban scale sealing with impervious materials affects the volume and velocity of runoff and results in flooding during intense rainfall (Skougaard Kaspersen et al. 2015). Over half of the world's population currently resides in urban areas, and this proportion is expected to increase by approximately 60% by 2030 (Nations et al. 2018). According to the report by European Environment Agency, various scenarios suggest that by the 2080s, an estimated 250,000 to 400,000 additional people per year in Europe will be impacted by floods, with a majority of them residing in urban areas (EEA 2020). In addition, many cities are expanding in size at an accelerated rate (Pathirana et al. 2014), and land use changes resulting from urbanization can have significant impacts on hydrometeorology due to modifications of surface and boundary layer atmospheric properties (Ren et al. 2008).

In a prior investigation, the correlation between rainfall and runoff in urban settings was examined, highlighting the adverse impact of population density and impervious surfaces on infiltration capacity. This analysis indicated a notable increase in flood magnitudes across sixteen drainage basins in Michigan (Brater and Sherrill 1975). Subsequently, (Darama 1985, 2000) conducted further research on the influence of impervious surfaces and urbanization on infiltration capacity within the same geographic region. These preceding studies collectively affirmed that the expansion of impervious surfaces diminishes infiltration capacity, consequently elevating the occurrence of flooding events. As a more recent study, Du et al. (2019) conducted a study to investigate the impact of varying urbanization levels on flooding in three cities located in the same river basin in

China. The study revealed that urbanization significantly increases the risk of flooding by causing an increase in peak flow and flood volume. (Wang et al. 2023) also studied the effect of urbanization on surface runoff by utilizing multiple scenario-based designs, correlation analysis, and a stepwise regression model. Findings indicate a significant increase in the conversion rate of rainfall to runoff when rainfall intensity reached 12.5 mm/12 h, highlighting an elevated waterlogging risk. Areas characterized by impervious surface proportions of 25–50% and 75–100% exhibited heightened sensitivity of surface runoff depth to increases in impervious surfaces, necessitating increased attention. It was determined that maintaining original high-density vegetation or augmenting vegetation density from 0–25 to 25–50% in urban green spaces is the most cost-effective approach. In addition, the arrangement and characteristics of the landscape, such as its fragmentation and shape, influence the quantity and depth of surface runoff. The excess impervious layer and its relationship with runoff have been the focus of interest for researchers recently (Prosdocimi et al. 2015; Du et al. 2019; Adetoro et al. 2022). In a different perspective, multi criteria decision making models such as Analytical Hierarchy Process (Demir et al. 2023; Demir and Dinçer 2023; Dinçer et al. 2023, 2024) have been used to assess the flood risks due to rapid urbanization and changing climate patterns (Nsangou et al. 2022; Waseem et al. 2023). In addition, studies on flood prevention determined the details of non-structural and structural measures (Ginige et al. 2022; Kreibich et al. 2015; WMO 2012). Furthermore, flood prevention methods integrated with ecology and environment have become prominent in recent years (Vojinovic et al. 2021). These methods, which are integrated with ecology and environment, are generally referred to as nature-based solutions (NBSs). The NBSs involve the increase of both pervious surfaces and the storage of runoff in basins, which are then released back into the natural environment. According to IPCC report, green roofs and permeable pavements are identified as NBSs for urban green space creation, reducing urban heat islands, mitigating the effects of global warming, and serving as an urban flood management strategy (IPCC 2022).

Pervious pavement has been the subject of numerous studies with respect to its impact on surface water quality and hydrologic characteristic (Thives et al. 2018; Alam et al. 2019). However, there are limited studies on its efficacy in reducing the extent of urban flood. Similarly, there have been many studies on the effects of rainfall intensity, substrate configuration, humidity, and the retention thickness and covered area of green roofs, as well as their aging, on reducing peak flow (Speak et al. 2013; Zhang et al. 2018, 2019; Liu et al. 2020). However, there are only a few studies on the effect of these parameters on reducing surface runoff. Despite these factors, the vast majority of studies revealed that green roofs are effective in reducing peak flow during storm events, with varying efficiency depending on the characteristics of the roofs and the study area (Sims et al. 2016; Zhang et al. 2018). The extent to which pervious pavement and green roofs can mitigate urban flooding has not been thoroughly studied.

The aim of this study is to investigate how excess urbanization, and the resulting reduction of pervious layers affect the extent of urban floods. To achieve this, a simulation of a flood event that occurred on September 22, 2022 in Erkilet District of Kayseri was conducted. To validate the hypothesis, which emerged from the field investigation suggesting that urbanization is the primary driver of flooding in the Erkilet District, the simulation was repeated on the topography of 2006. The results confirmed that urbanization is indeed one of the main causes of flooding in the area. Furthermore, the effectiveness of green roofs and permeable pavements as NBSs for increasing the permeability of urban areas and mitigating floods was analyzed. The study solidly demonstrates the impact of excessive urbanization, occurring in the 16-year period, on the occurrence of urban

flood and to concretely put forth the degree to which the application of green roofs and permeable pavement, considered as NBSs, is effective in reducing the adverse effects of floods. The novelty of our study lies in its exploration of the impact of urbanization on flooding and the effectiveness of green roofs and permeable pavements in reducing surface runoff. While previous literature has extensively investigated these factors separately, our study uniquely assesses their combined effect on a flood event and its extent, a perspective that has not been explored before.

## 2 The study area

The study area is situated approximately 10 km north of Kayseri city center, a major metropolitan city in central Anatolia and in close proximity to Türkiye's capital, Ankara. Erkiilet experiences a dry climate during the summer season, while mild precipitation is observed during the winter months. Erkiilet's climate sees temperatures typically ranging between  $-8\text{ }^{\circ}\text{C}$  and  $29\text{ }^{\circ}\text{C}$  throughout the year, occasionally dipping below  $-16\text{ }^{\circ}\text{C}$  or rising above  $34\text{ }^{\circ}\text{C}$ . Rainfall days vary throughout the year, defined as days with at least 1 mm of liquid or liquid-equivalent precipitation in Erkiilet. The rainy season extends for 8.2 months, from October 15th to June 20th, with a probability of any given day being rainy at over 13%. May registers the highest average rainfall, with an average of 6.6 days experiencing at least 1 mm of rainfall. In contrast, the dry season commences on June 20th and spans 3.8 months until October 15th. Precipitation types are categorized into solely rain, solely snow, or a mix of both, with their prevalence varying throughout the year in Erkiilet. Solely rain predominates for 11 months, commencing from February 12th to January 3rd, with May having the highest number of solely rainy days, averaging 6.5 days. Snow is most common for 1.1 months, starting from January 3rd to February 7th, with January experiencing the highest number of solely snowy days, averaging 1.8 days. A mix of rain and snow is most frequent for 5.0 days, beginning from February 7th to February 12th, with February having the highest number of mixed precipitation days, averaging 1.4 days. Erkiilet exhibits some seasonal variations in monthly rainfall amounts. The rainy period of the year, with a minimum of 13 mm of moving 31-day rainfall amount, spans 9.4 months from September 24th to July 5th, with May being the rainiest month in Erkiilet, boasting an average rainfall of 35 mm. The long-term average annual precipitation recorded from 1991 to 2020 by the Turkish State Meteorological Service (MGM) is 390.2 mm (MGM 2023). These climatic conditions and geographical location are detailed in Fig. 1, which provides information on watersheds, drainage lines, the computational domain, and control points used for examining flow depths in various scenarios.

## 3 Methodology

The aim of this study is to put forth the detrimental effect of urbanization on urban flood regarding historical flood event, and to evaluate the effectiveness of green roofs and pervious pavement in mitigating the negative impacts of the historical flood. To achieve this, relevant data was acquired to simulate the existing flood event that occurred on September 22, 2022, in Erkiilet District of Kayseri province, Türkiye. The hourly precipitation over Erkiilet on September 22 was obtained from the ERA-5 reanalysis product, a multi-dimensional raster with proven accuracy for global and nationwide

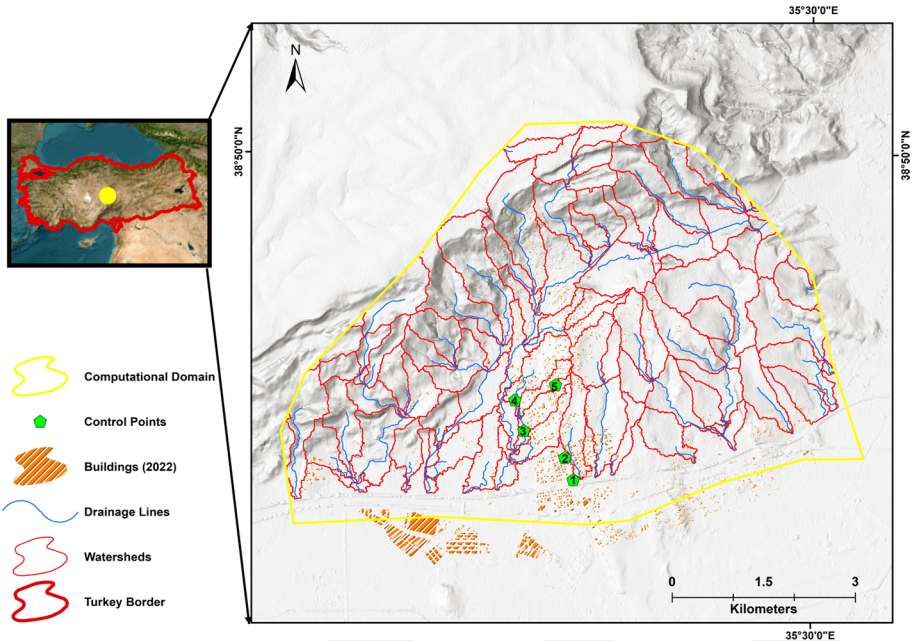


**Fig. 1** The study area and computational domain

extent (Hersbach et al. 2020; Bell et al. 2021). Furthermore, to investigate the impact of urbanization on floods, the study utilized satellite imagery to reconstruct the building and topographic characteristics of the study area as it existed in 2006.

Fieldwork was carried out to analyze soil samples from 10 locations, accurately determining the soil structure and permeability of the area. The geometric features of hydraulic structures such as bridges, culverts, and decks, as well as their coordinates, were also determined. The Metropolitan Municipality of Kayseri provided vector data of buildings, roads, and other features, as well as a digital elevation model (DEM) of the region. The surface roughness of the study area was determined by considering land use classes of CORINE 2018 and CORINE 2006. All the obtained and processed data were used to implement a hydraulic model for simulating the urban flood that occurred on September 22, 2022.

To calibrate the model, variables such as water depth and flood propagation velocity, which were not recorded by institutions, were determined through field studies. After simulating the urban flood event, the implementation of green roofs and pervious pavements as a mitigation measure was analyzed, and changes in flood propagation and hazard classes were determined. A detailed flow chart of the study is presented in Fig. 2.

### 3.1 Geotechnical characteristics and field study

The case study area has undergone rapid and intense urbanization over the past decade, leading to a considerable decrease in the ratio of free fields to the total area. This has resulted in a significant reduction in the area's water absorption capacity. Thus, it was crucial to determine the soil properties of the area, along with its potential water absorption

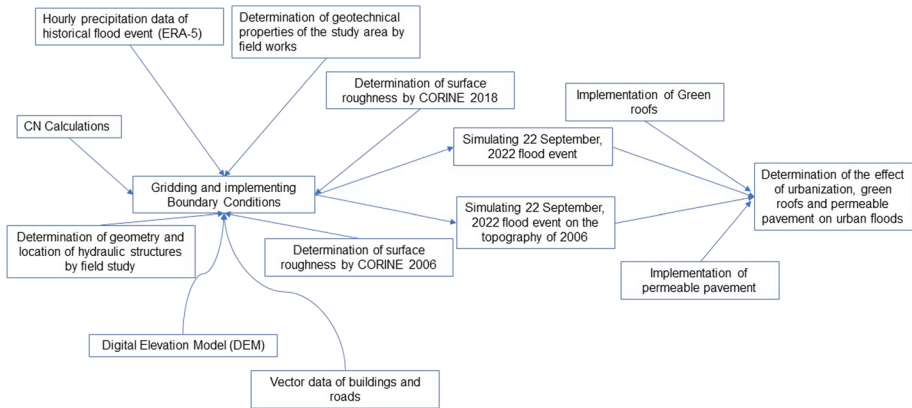


**Fig. 2** Flowchart of the study

capacity. To achieve this, a comprehensive study was conducted, which included both site surveys and laboratory experiments.

### 3.1.1 Soil sampling

To delineate suitable sampling sites within the designated area, an observational site survey was undertaken. This survey, supplemented by consultations with local experts, facilitated the identification of potential zones where soil characteristics are likely to exhibit variability. Accordingly, ten locations were selected, distributed across the entire area (see Fig. 3). From each of these locations, two disturbed samples were collected for sieve analysis, water content ( $W_n$ ), and consistency limit experiments. In addition, at five of these ten locations, soil samples were taken using a steel thin-walled sampler to determine the in-situ relative density. The data from these samples were used to calculate the in-situ natural unit weight ( $\gamma_n$ ) of the soil to determine the water absorption capacities of the samples.

### 3.1.2 Laboratory studies

After being collected from the investigated area, the samples were sealed and transported to the Geotechnics Laboratory of Çankaya University's Civil Engineering Department. At each location, each test was repeated twice (once for each sample) to ensure accuracy. The results of these experiments were found to be reasonably similar, with a margin of error of  $\pm 5\%$ . Therefore, the average of the two tests was taken as the representative value for each sample location.

To obtain the particle size distribution curves, sieve analysis tests were conducted in accordance with ASTM D 422–63 (2007) on all samples. Particle size distribution curves of 4 representative samples were presented in Fig. 4 where it can be seen that the curves obtained from both samples at each presented location show similar characteristics. Accordingly, the average particle size distribution curves were obtained for each sample location and given in Fig. 5. All samples were classified as poorly graded sand “SP” according to ASTM D 2487 (2017) with a fines content lower than  $FC < 5\%$ .

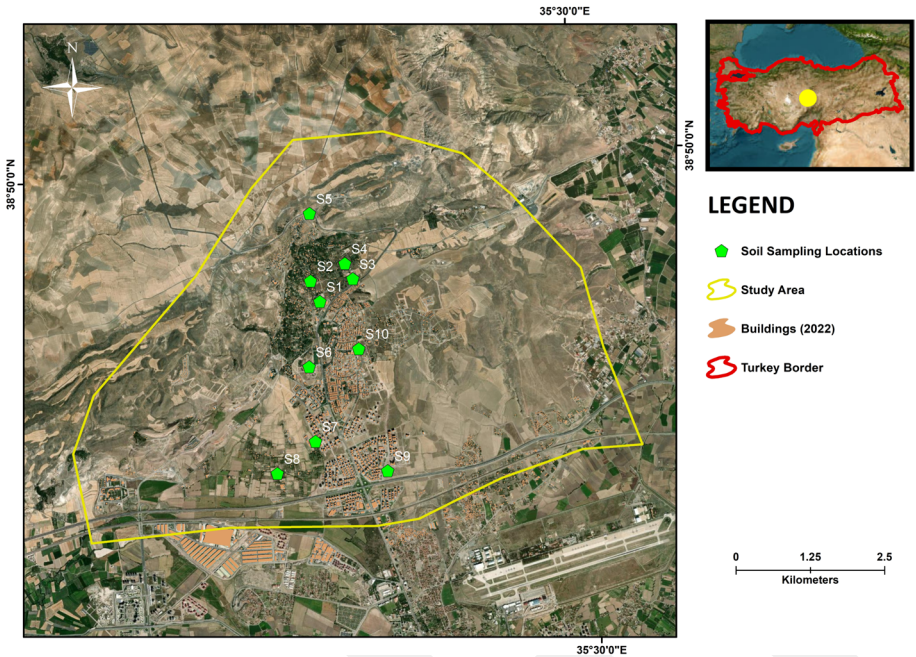


Fig. 3 Soil sample locations

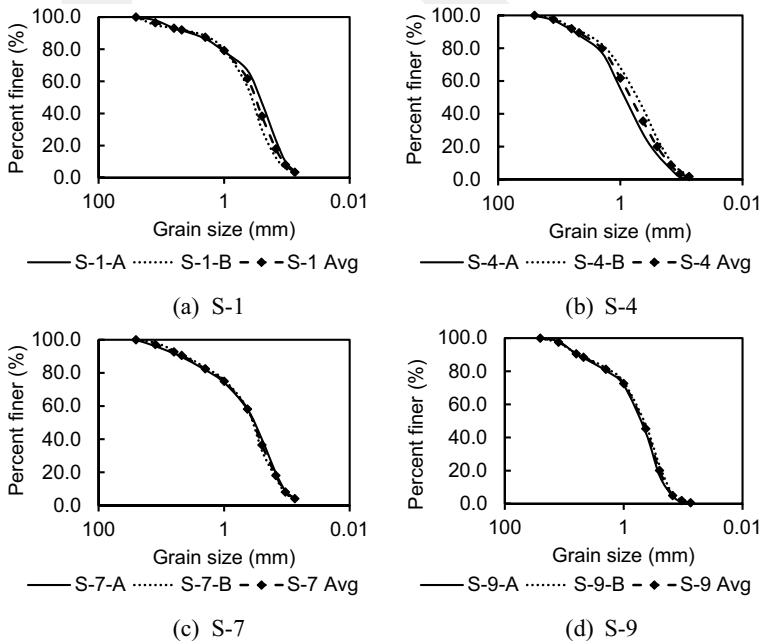
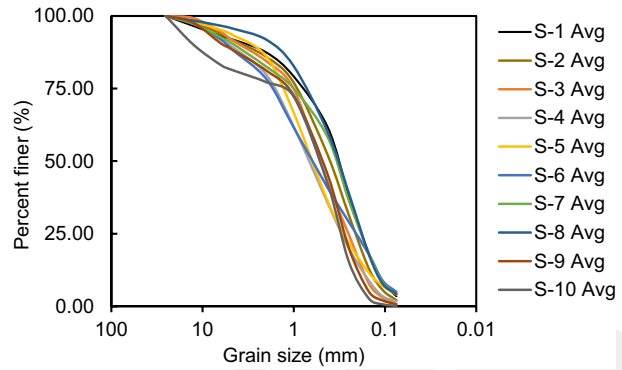


Fig. 4 Separate and average particle size distribution curves for selected locations

**Fig. 5** Average particle size distribution curves



Consistency limit tests were conducted according to ASTM D 4318 (2010), and the tested samples were found to be non-plastic (NP). The natural water contents of the samples were obtained according to ASTM D 2216 (2019) and were found to vary within the range of 9.06–20.94% for the tested samples. The basic soil properties of the tested samples are summarized in Table 1.

The water absorption capacities of the soil samples were determined by utilizing the test results obtained. To accomplish this, the natural unit weight ( $\gamma_n$ ), natural water content ( $W_n$ ), and specific gravity ( $G_s$ ) of the soil samples extracted by steel thin-walled samplers were initially ascertained following the guidelines provided by ASTM D 7263 (2021), ASTM D 2216 (2019), and ASTM D 854 (2014), respectively. Subsequently, the in-situ void ratio ( $e$ ) and degree of saturation ( $S_{rn}$ ) values were calculated utilizing the following equations.

$$\gamma_{dry} = \frac{\gamma_n}{(1 + w_n)} \quad (1)$$

$$\gamma_{dry} = \frac{G_s * \rho_w}{(1 + e)} \quad (2)$$

**Table 1** Soil classification and basic properties of tested samples

Soil sample	D <sub>60</sub>	D <sub>30</sub>	D <sub>10</sub>	FC (%)	Cu	Cc	Soil Class	Plasticity	W <sub>n</sub> (%)
S-1	0.42	0.20	0.13	3.45	3.23	0.73	SP	NP	14.53
S-2	0.55	0.26	0.15	2.08	3.67	0.82	SP	NP	14.94
S-3	0.68	0.30	0.17	0.71	4.00	0.78	SP	NP	13.56
S-4	0.98	0.37	0.16	1.72	6.13	0.87	SP	NP	20.94
S-5	0.80	0.35	0.14	4.08	5.71	1.09	SP	NP	19.49
S-6	0.98	0.26	0.12	4.95	8.17	0.57	SP	NP	15.99
S-7	0.48	0.21	0.12	4.14	4.00	0.77	SP	NP	14.30
S-8	0.42	0.20	0.13	4.28	3.23	0.73	SP	NP	12.11
S-9	0.66	0.30	0.19	0.64	3.47	0.72	SP	NP	12.02
S-10	0.68	0.33	0.20	0.12	3.40	0.80	SP	NP	9.06

$$e * S_{rn} = w_n * G_s \quad (3)$$

The degree of saturation ( $S_{rn}$ ) of the soil samples in their natural state was determined by utilizing equations Eq. (1–3). As all of the tested soil samples were identified as non-plastic poorly graded sands (SP), their maximum water absorption capacities are restricted to the amount of water that can be absorbed from their natural (partially saturated) state to a fully saturated state ( $S_r=1$ ). In addition, the depth of the partially saturated soil ( $D_{PSS}$ ) was measured at each sampling location by excavating the ground until a relatively wet soil layer was visible, and " $D_{PSS}$ " was defined as the distance from the ground surface to the uppermost level of this relatively wet soil layer. Finally, the total amount of water absorption per square meter of surface area ( $W_{AC}$ ) was determined by utilizing Eqs. (4) and (5), which are presented below.

$$e * (S_r = 1) = w * G_s \quad (4)$$

$$W_{AC} = \frac{(w - w_n) * \gamma_{dry}}{9.81 * 100} \quad (5)$$

The related test results and the resulting water absorption capacities ( $W_{AC}$ ) of the tested samples are summarized in Table 2.

## 4 Summary of field and geotechnical studies

The site surveys revealed that the soil profile of the investigated area could be categorized into four primary regions, with "Erkilet Boulevard" serving as a natural boundary between them (Fig. 6). In "Region 1," the depth of the partially saturated soil was measured to be  $D_{PSS} \approx 40\text{--}60$  cm, and the soil profile beneath this depth was predominantly composed of sandy soil layers. Most of the open areas in "Region 1" are currently being used as agricultural land. However, in "Region 2," the  $D_{PSS}$  was measured to be  $D_{PSS} \approx 30$  cm, and a significant difference from "Region 1" was that rocky layers were observed beneath the surficial soil layer. Additionally, these rocky layers were observed to come to the surface at a short distance, resulting in  $D_{PSS} \approx 0$  cm, which was defined as the boundary between "Region 2—Region 3" (Fig. 7). As a result, the water absorption capacity of "Region 3" is practically zero, since there is no surficial soil. In "Region 3," there is a small area covered with a 10 cm thick surficial soil. Although the  $W_{AC}$  of this region is limited due to its small area and  $D_{PSS}$ , it is still evaluated separately as "Region 4" to account for all possible water absorption in the investigated area.

### 4.1 Hydrologic characteristics

The re-analysis product of ERA-5 was used to obtain precipitation data for the rainfall event that occurred on September 22, 2022. The obtained precipitation data is visually represented in Fig. 8.

The obtained precipitation data serves as a gridded boundary condition for the hydraulic model, enabling the simulation of the flood event. However, to determine the surface runoff generated by the rainfall, it is necessary to have information regarding the permeability and curve number of the region. To achieve this, the study area

**Table 2** Absorption capacities of the tested soil samples

Soil sample	$\gamma_n$ (kN/m <sup>3</sup> )	$W_n$ (%)	$\gamma_{dry}$ (kN/m <sup>3</sup> )	$G_s$	$e$ (%)	$S_r$ (%)	$w$ ( $S_r = 1$ )	$D_{pss}$ (m)	$W_{AC}$ (m <sup>3</sup> )	$W_{AC}$ (kg/m <sup>2</sup> )
S-1	17.41	14.53	15.20	2.58	0.67	56.36	25.78	0.60	0.10	105
S-3	18.44	13.56	16.24	2.64	0.59	60.19	22.53	0.60	0.09	89
S-7	17.65	14.30	15.44	2.60	0.65	57.06	25.06	0.40	0.07	68
S-8	16.90	12.11	15.08	2.55	0.66	46.86	25.85	0.40	0.08	84
S-10	17.63	9.06	16.16	2.61	0.58	40.51	22.37	0.10	0.02	22

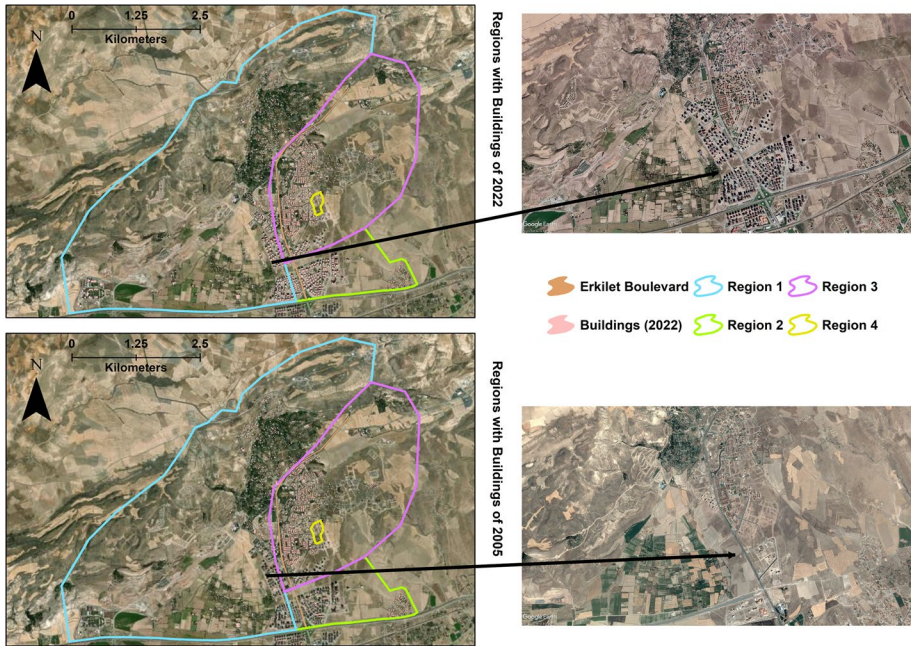


**Fig. 6** Regions of Erketilet according to  $W_{AC}$

**Fig. 7** The border of Region 2 – Region 3



was divided into polygons as shown in Fig. 9 based on considerations such as land use classes, geotechnical studies conducted in the field, and the presence of buildings, roads, and other features for both the simulation years of 2006 and 2022. In the figure buildings are represented by yellow dots. The figure distinctly illustrates the degree of urbanization between 2006 and 2022.

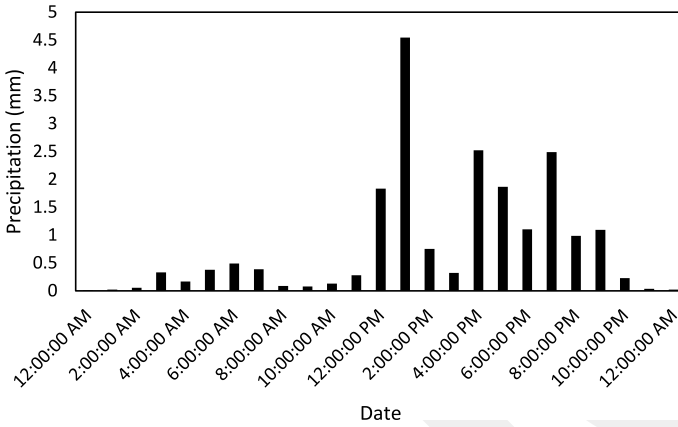


Fig. 8 Satellite precipitation data of September 22, 2022 on Erketil (ERA-5 reanalysis product)

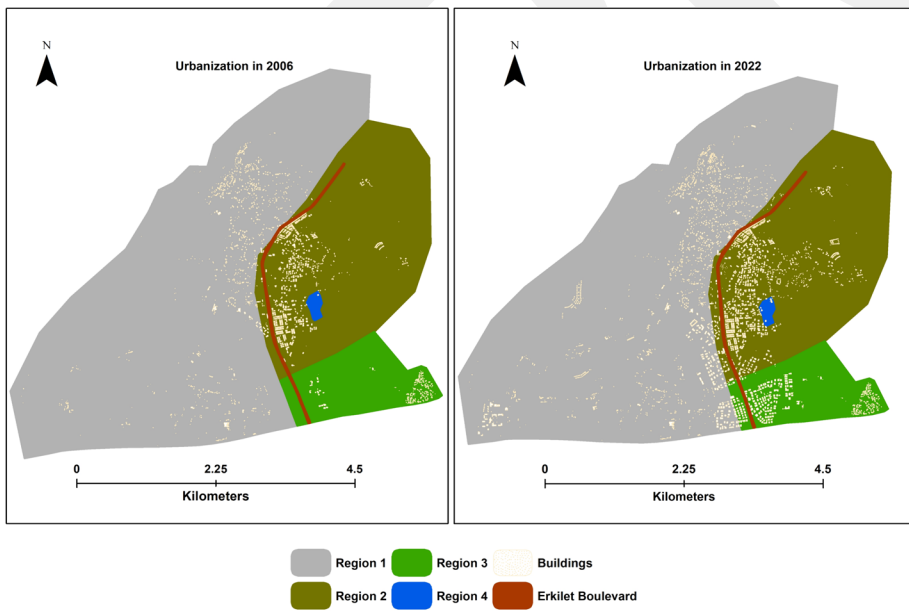


Fig. 9 Hydrologic characteristics of the study area

### 4.2 Hydraulic model

In this study, the excess precipitation and corresponding surface flow of the Erketil District on 22nd September 2022 was simulated by implementing an unsteady 2D HEC-RAS model. The governing equations for solving the 2D unsteady flow throughout the computational domain are given below.

$$\frac{\partial h}{\partial t} + \frac{\partial(hu)}{\partial x} + \frac{\partial(hv)}{\partial y} = q \tag{6}$$

$$\frac{\partial u}{\partial t} + u \frac{\partial u}{\partial x} + v \frac{\partial u}{\partial y} - f_c v + g \frac{\partial Z_s}{\partial x} - \frac{1}{h} \frac{\partial}{\partial x} \left( v_{t,xx} h \frac{\partial u}{\partial x} \right) - \frac{1}{h} \frac{\partial}{\partial y} \left( v_{t,yy} h \frac{\partial u}{\partial y} \right) = \frac{\tau_{b,x}}{\rho R} + \frac{\tau_{s,x}}{\rho h} \tag{7}$$

$$\frac{\partial v}{\partial t} + u \frac{\partial v}{\partial x} + v \frac{\partial v}{\partial y} - f_c u + g \frac{\partial Z_s}{\partial y} - \frac{1}{h} \frac{\partial}{\partial x} \left( v_{t,xx} h \frac{\partial v}{\partial x} \right) - \frac{1}{h} \frac{\partial}{\partial y} \left( v_{t,yy} h \frac{\partial v}{\partial y} \right) = \frac{\tau_{b,y}}{\rho R} + \frac{\tau_{s,y}}{\rho h} \tag{8}$$

where  $u$  and  $v$  are the velocities in the  $x$  and  $y$  coordinates,  $g$  is the gravitational acceleration,  $Z_s$  is the water surface elevation,  $v_{t,xx}$  is the horizontal eddy viscosity,  $\tau_{b,x}$  is the bottom shear stress,  $R$  is the hydraulic radius,  $\tau_{s,x}$  is the wind stresses,  $h$  is the water depth, and  $f$  is the Coriolis parameter.

When the flow is primarily dominated by gravity and friction forces, a simplified form of Shallow Water Equations (SWEs), known as Diffusion Wave Approximation or Diffusive Wave Equations (DWEs), can be implemented as the governing equations. During the derivation of DWEs, the local and convective acceleration terms were excluded from the SWEs, considering the domination of gravity and friction forces. As a result, the momentum equations of DWEs can be expressed as follows:

$$g \frac{\partial Z_s}{\partial x} - \frac{1}{h} \frac{\partial}{\partial x} \left( v_{t,xx} h \frac{\partial u}{\partial x} \right) - \frac{1}{h} \frac{\partial}{\partial y} \left( v_{t,yy} h \frac{\partial u}{\partial y} \right) = \frac{\tau_{b,x}}{\rho R} \tag{9}$$

$$g \frac{\partial Z_s}{\partial y} - \frac{1}{h} \frac{\partial}{\partial x} \left( v_{t,xx} h \frac{\partial v}{\partial x} \right) - \frac{1}{h} \frac{\partial}{\partial y} \left( v_{t,yy} h \frac{\partial v}{\partial y} \right) = \frac{\tau_{b,y}}{\rho R} \tag{10}$$

In the analysis employed in the current study, it is notable that the flow dynamics are principally governed by gravitational and frictional forces (Darama et al. 2021; Yılmaz et al. 2023a). Consequently, DWEs were selected as the appropriate numerical tool.

The gridding process and boundary conditions of the hydraulic model are depicted in Fig. 10. The computational domain utilizes a maximum grid size of 10 m, while smaller grids of up to 1 m are employed to cover roads, rivers, and culverts. The regions in which refined grids are employed are also shown in Fig. 10.

To allow excess water to exit the computational domain, a normal depth boundary condition is selected with a slope of 0.0008. The determination of these normal depth values is based on an examination of the topographic data of the study area.

### 4.2.1 Digital elevation model (DEM)

The DEM, which has a 5-m resolution and is presented in Fig. 11, was provided by the Greater Municipality of Kayseri in a TIN format and subsequently converted to raster format. In order to obtain the geometric properties of buildings, such as their total area and locations, a satellite view from 2006 and 2022 was assessed. The buildings were then integrated into the DEM prior to implementing the hydraulic model. The buildings 2006 and 2022 can be clearly seen in both DEMs shown in Fig. 11.



Fig. 10 Study area grids used in hydraulic model

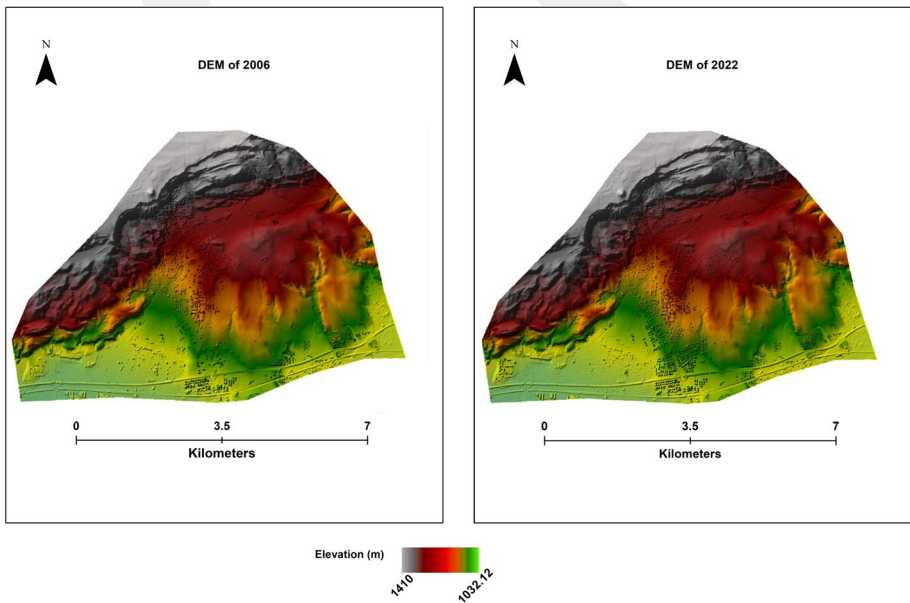


Fig. 11 Digital elevation model of the study area for 2006 and 2022

### 4.2.2 Surface roughness

Surface roughness is a critical variable in calibrating a hydraulic model. Therefore, the determination of roughness is of utmost importance. Typically, the calibration process involves examining field data from historical events or evaluating data from gauging stations. However, there are no gauging stations in the study area that could be used to determine roughness based on land cover. To address this limitation, the computational area was classified according to the land-use data of CORINE 2018 for simulating the hydraulic model of 2022 while land-use data of CORINE 2006 was used for simulating hydraulic model of 2006, as illustrated in Fig. 12. Notably, the figure vividly illustrates the discernible expansion of the urban area marked in red over time.

Table 3 presents the average values of surface roughness coefficients for the study area based on the land cover classification. These coefficients were determined using a study conducted by Papaioannou et al. (2018), which utilizes the CORINE 2018 land cover data to establish surface roughness coefficients for each specific land cover type.

### 4.3 Scenarios

The primary objective of developing scenarios is to create a depiction of an excessively urbanized area during heavy precipitation, the conditions of the pre-urbanized area, and the impact of nature-based solutions (NBS) on reducing the adverse effects of surface runoff. To achieve this goal, five different scenarios were developed, and presented in Table 4. Scenario 1 (Sc-1) focuses on the urbanized era, specifically examining the flood event

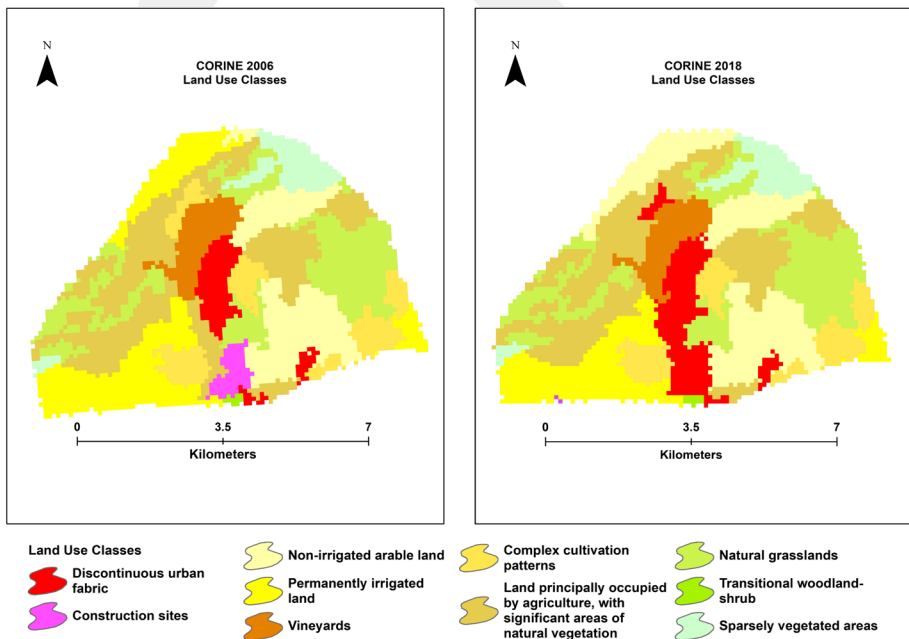


Fig. 12 Land cover classification of the computational domain according to CORINE 2006 and CORINE 2018

**Table 3** Variation of surface roughness with respect to land cover for the computational domain (Papaioannou et al. 2018)

Land use classes	Surface roughness
Discontinuous urban fabric	0.013
Industrial, commercial units	0.013
Construction Sites	0.013
Non-irrigated arable land	0.03
Permanently irrigated land	0.03
Vineyards	0.08
Complex cultivation patterns	0.04
Land principally occupied by agriculture, with significant areas of natural vegetation	0.05
Natural grassland	0.04
Transitional woodland / shrub	0.06
Sparsely vegetated areas	0.027

**Table 4** Scenarios under varying physical condition

Scenario #	Explanation
Sc-1	Urbanized Era – The Flood Event of September 22, 2022
Sc-2	Pre-Urbanized Era of 2006
Sc-3	Implementation of Green Roofs to Sc-1
Sc-4	Implementation of Permeable Pavement to Sc-1
Sc-5	Implementation of Green Roofs and Permeable Pavement to Sc-1

occurred on September 22, 2022. Scenario 2 (Sc-2) represents the pre-urbanized era of 2006, offering insights into conditions prior to significant urbanization. Scenarios 3, 4, and 5 (Sc-3, Sc-4, Sc-5) involve the implementation of green roofs, permeable pavement, and a combination of both, respectively, in Sc-1.

## 5 Results and discussion

### 5.1 Permeability and curve number calculations

The constructed polygons shown in Fig. 9 were incorporated into the hydraulic model to define the permeability and curve number (CN) of each region. The permeability and CN values for each region were calculated, taking into account the field study and land use classes, and are presented in Tables 5 and 6. It is important to mention that the calculations excluded the area occupied by buildings and Erkilet Boulevard. However, the CN values for buildings and Erkilet Boulevard were assumed to be 98 consistent with the suggestions in (Feldman 2000). Green roofs and permeable pavements were obviously excluded from the calculations presented in Tables 5 and 6.

The CN and permeability values for green roofs and permeable pavement were established based on existing literature (Andersen et al. 1999; Collins et al. 2008; Schwartz

**Table 5** CN calculations for 2022

Region 1 – (A Group Soil)				Region 2 – (B Group Soil)			
Area (km <sup>2</sup> )	CORINE CODE	Area ratio (%)	CN	Area (km <sup>2</sup> )	CORINE CODE	Area ratio (%)	CN
0.88	112	5.07	68	0.62	112	28.96	98
0.27	211	1.58	77	1.18	211	55.31	86
3.06	212	17.67	74	0.34	321	15.74	79
2.14	221	12.37	58				
1.05	242	6.04	64				
6.62	243	38.21	74				
2.68	321	15.44	39				
0.63	333	3.62	68				
Region—1 CN Average:			65.54	Region—2 CN Average			88.37
Region 3 – (C Group Soil)				Region 4 – (D Group Soil)			
Area (km <sup>2</sup> )	CORINE CODE	Area ratio (%)	CN	Area (km <sup>2</sup> )	CORINE CODE	Area ratio (%)	CN
1.65	112	22.22	98	0.03	242	50.00	82
1.99	211	26.70	94	0.03	321	50.00	79
0.10	221	1.29	84				
0.74	242	9.96	85				
1.89	243	25.40	90				
0.89	321	11.99	84				
0.18	333	2.44	89				
Region—3 CN Average:			91.53	Region—4 CN Average:			80.50

**Table 6** CN calculation for 2006

Region 1 – (A Group Soil)				Region 2 – (B Group Soil)			
Area (km <sup>2</sup> )	CORINE CODE	Area Ratio (%)	CN	Area (m <sup>2</sup> )	CORINE CODE	Area Ratio (%)	CN
0.07	112	0.43	68	0.12	112	5.75	98
0.01	133	0.09	98	0.40	133	19.02	98
0.03	211	0.17	77	1.21	211	56.89	86
3.33	212	19.28	74	0.07	243	3.36	79
2.12	221	12.24	58	0.32	321	14.98	79
1.54	242	8.91	64				
6.84	243	39.59	74				
2.71	321	15.65	39				
0.63	333	3.64	68				
Region—1 CN Average:			65.45	Region—2 CN Average:			87.69
Region 3 – (C Group Soil)				Region 4 – (D Group Soil)			
Area (km <sup>2</sup> )	CORINE CODE	Area Ratio (%)	CN	Area (km <sup>2</sup> )	CORINE CODE	Area Ratio (%)	CN
1.57	112	20.92	98	0.04	242	56.52	82
2.01	211	26.71	94	0.04	321	41.45	79
0.08	221	1.11	84	0.001	112	2.04	98
0.76	242	10.12	85				
1.98	243	26.36	90				
0.91	321	12.07	84				
0.20	333	2.72	89				
Region—3 CN Average:			91.42	Region—4 CN Average:			81.08

2010; Liu et al. 2020). Previous research indicates that the CN for green roofs is 93 and for permeable pavement is 75, while their respective permeability rates are 50% and 65%.

## 5.2 Effect of urbanization on urban flooding

To ascertain whether excess urbanization is the main driver of urban flooding over a 16-year period, a comparison is conducted between Sc-1 and Sc-2. Sc-1 represents the current state of excessive urbanization, while Sc-2 depicts the pre-urbanization conditions.

Although the grid size and boundary conditions remain consistent across scenarios, there is a discrepancy in computational time. This disparity can be attributed to the inclusion of CN and permeability calculations, which introduce additional computational complexities into the models.

Figure 13 shows the flood inundation for the topography of 2006 and 2022 on a land use map. The figure illustrates that the overall inundated area does not exhibit a significant difference in the case of excessive urbanization. However, the primary disparity arises within the urbanized region. The excess urbanization extent the inundation area, causing excess flood water out of the urbanized area (Fig. 13a). Furthermore, the excess urbanization also caused flood water to reach the regions that should not be inundated

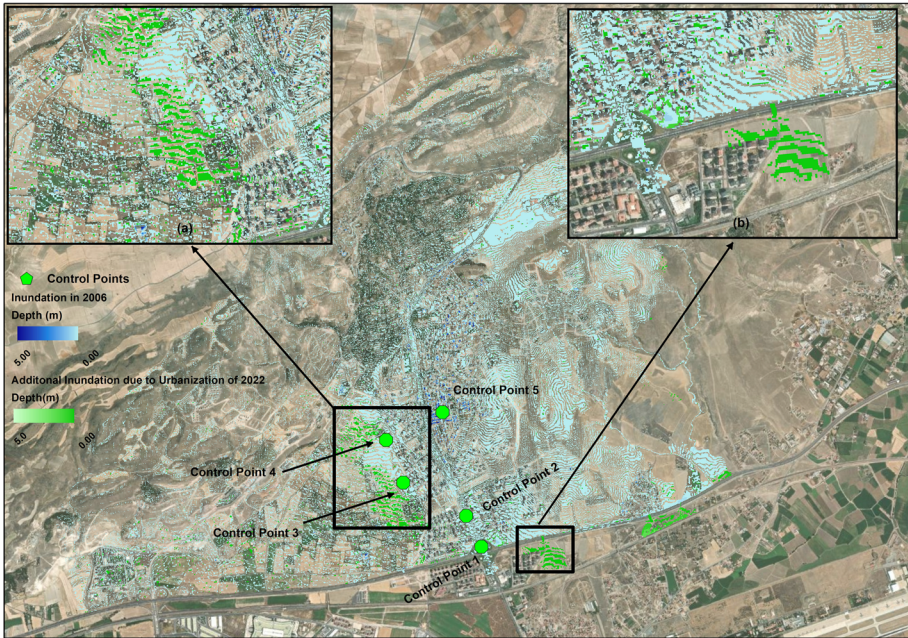


**Fig. 13** Effect of urbanization on flood (Sc-1 vs Sc-2)

if the urbanization does not take place (Fig. 13ab). To further assess the variations between the two scenarios, Table 7 presents the water depths at the pre-defined control points. This allows for a detailed examination of the discrepancies between the scenarios in terms of water depth measurements.

The analysis of water depths at the control points reveals notable discrepancies in flow depths between the two different topographies representing the years 2006 and 2022, particularly in the urbanized area. The increase in flow depth ranges from approximately 9.8% up to 195%. These findings from the simulation provide concrete evidence that the impacts of the historical flood’s precipitation event would have been less significant if it had occurred during the pre-urbanized era of 2006.

**Table 7** Flow depth at the control points

Control point #	Sc-1 depth (cm)	Sc-2 depth (cm)	Difference (%)
1	10.40	8.09	28.51
2	2.80	2.12	31.61
3	7.68	2.60	195.30
4	6.86	6.25	9.76
5	16.13	9.67	66.79

### 5.3 Effect of green roofs and permeable pavements on flood mitigation

In Sc-3, all the roofs within the computational domain are replaced by green roofs, assuming they have the same permeability and water retention capacity. This scenario focuses exclusively on the implementation of green roofs as a nature-based solution. In Sc-4, the assumption is made that Erkilet Boulevard is covered with permeable pavement. This scenario specifically investigates the effects of permeable pavement as a mitigation measure. Lastly, in Sc-5, the assumptions made in both Sc-3 and Sc-4 are simultaneously applied. This scenario combines the implementation of green roofs and permeable pavement to assess the combined effectiveness of these nature-based solutions.

Figure 14 provides insights into the effectiveness of different measures in reducing floodwater depths. The results indicate that green roofs are capable of mitigating flood risks by reducing water depths by up to 4%. Similarly, permeable pavement contributes to the reduction of total surface runoff depth up to 5.2%.

When both green roofs and permeable pavement are implemented together, the combined approach proves to be slightly more effective, reducing flow depths up to 6.2%.

It is important to note that while increasing the pervious layer through nature-based solutions (NBS) in urbanized areas can help reduce the adverse effects of floods, the extent of their effectiveness is limited. Therefore, structural measures remain crucial and should be complemented and supported by the implementation of NBSs.

## 6 Discussions

Numerous studies have indicated that urbanization plays a prominent role in the escalation of flood events (Yang et al. 2013; Shao et al. 2020). Supporting this notion, a report by the European Environment Agency (EEA) in 2020 highlighted a correlation between increased urbanization and elevated flood flows (EEA 2020). Furthermore, research examining flooding patterns in the Xiang River Basin by Du et al. (2019) demonstrated a direct relationship between urbanization levels and peak flood flows, revealing that the ratio of peak floods incrementally corresponds to urbanization percentages. A study conducted in Ayamama Watershed, Istanbul, Türkiye, by Nigussie and Altunkaynak (2019) similarly affirmed

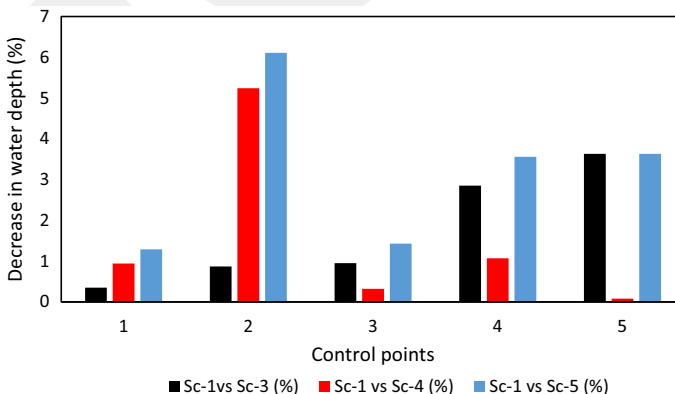


**Fig. 14** The decrease in water depths due to NBSs

that unrestricted urbanization leads to an expansion of flood inundation areas. In alignment with these prior investigations, our study in the Erkilet area confirmed that excessive urbanization results in inundation areas and flow depths up to 195% higher as depicted in Fig. 13 and in Table 7.

On a distinct note, NBSs for flood prevention involve the strategic use of natural features and processes to manage and mitigate flooding (Slinger et al. 2023). The efficacy of NBSs in reducing flood risks has been extensively discussed in previous research. According to a comprehensive review conducted by Huang et al. (2020), NBSs exhibit significant effectiveness in mitigating urban flooding triggered by high-frequency precipitation events, offering additional economic, ecological, and social advantages. However, NBSs have limitations in addressing pluvial flooding resulting from intense, short-term precipitation events, while conventional gray infrastructure also faces constraints as a mitigation measure against extreme flooding. In congruence with existing literature, our study underscores that the effectiveness of NBSs in the case study area is constrained primarily due to the relatively small area allocated for permeable pavement and green roofs. Notably, the reduction in water depths achieved by NBSs in the best-case scenario is 6.2%, highlighting the need to identify flood risk management strategies by evaluating the performance of alternative combinations of NBSs with gray infrastructure in the context of flood prevention within urban areas.

The significance of this study lies in its capacity to demonstrate the ramifications of excessive urbanization on flood risks and to assess whether the combinations of NBSs can serve as a viable solution to counteract the increased flood risks associated with urbanization.

## 7 Conclusions

Urbanization has been observed to have a detrimental impact on urban flooding, leading to an increased frequency of peak floods and larger areas of inundation due to the reduction of pervious layers. This trend is expected to worsen in the face of population growth and global warming, which contribute to more frequent and severe hydrometeorological extremes. Therefore, the aim of this study is to prove the effect of urbanization on urban flooding by simulating a flood event that occurred in Erkilet, Kayseri on September 22, 2022, and comparing it with the pre-urbanized conditions of the same region. Furthermore, the effectiveness of NBSs in mitigating urban flooding is also explored.

The results of the study confirm that urbanization has indeed increased the risk of flooding by reducing the availability of pervious surfaces. However, the implementation of green roofs has shown promise in reducing urban flooding and associated flood hazards, with the extent of reduction depending on the configuration of the green roofs, which directly affects the curve number. Regardless of the specific curve number or roof configuration, there was a decrease in flood hazard ranging from 1 to 5% throughout the rainfall event. Similarly, the use of permeable pavements has also demonstrated its effectiveness in reducing urban flooding and associated flood hazards, depending on the configuration of the pavements and their impact on the curve number. The implementation of permeable pavements resulted in a reduction in peak flow discharges and flood hazards. Moreover, when both green roofs and permeable pavements were combined, there was a further reduction in peak discharges. However, it is important to note that nature-based

solutions alone are not sufficient to completely prevent floods. They should be considered as supporting measures alongside gray infrastructure as literature suggests.

**Author contributions** “Şevki Öztürk: Conceptualization, Investigation, Funding Acquisition, Writing—Review & Editing Ali Ersin Dinçer: Conceptualization, Investigation, Writing—Review & Editing, Funding Acquisition Kutay Yılmaz: Conceptualization, Methodology, Validation, Formal Analysis, Writing—Original Draft, Writing—Review & Editing Volkan Kalpakçı: Conceptualization, Investigation, Writing—Review & Editing, Funding Acquisition”.

**Funding** Open access funding provided by the Scientific and Technological Research Council of Türkiye (TÜBİTAK). We would like to acknowledge the partial funding provided for the fieldwork by The Scientific and Technological Research Council of Türkiye (TÜBİTAK) “1002-C Natural Disasters-Focused Fieldwork Emergency Support Program (Doğal Afetler Odaklı Saha Çalışması Acil Destek Programı)”.

## Declarations

**Conflict of interest** The authors have no relevant financial or non-financial interests to disclose.

**Open Access** This article is licensed under a Creative Commons Attribution 4.0 International License, which permits use, sharing, adaptation, distribution and reproduction in any medium or format, as long as you give appropriate credit to the original author(s) and the source, provide a link to the Creative Commons licence, and indicate if changes were made. The images or other third party material in this article are included in the article’s Creative Commons licence, unless indicated otherwise in a credit line to the material. If material is not included in the article’s Creative Commons licence and your intended use is not permitted by statutory regulation or exceeds the permitted use, you will need to obtain permission directly from the copyright holder. To view a copy of this licence, visit <http://creativecommons.org/licenses/by/4.0/>.

## References

- Adetoro O-IO, Osarenren V, Popoola SO (2022) Effects of increasing impervious surface on water quality in Ile-Ife urban watershed, Southwestern Nigeria. *J Geosci Environ Protect* 10:126–160. <https://doi.org/10.4236/gep.2022.1012010>
- Alam T, Mahmoud A, Jones KD et al (2019) A comparison of three types of permeable pavements for urban runoff mitigation in the semi-arid South Texas USA. *Water (switzerland)*. <https://doi.org/10.3390/w11101992>
- Alfieri L, Bisselink B, Dottori F et al (2017) Global projections of river flood risk in a warmer world. *Earths Future* 5:171–182. <https://doi.org/10.1002/2016EF000485>
- Andersen CT, Foster IDL, Pratt CJ (1999) The role of urban surfaces (permeable pavements) in regulating drainage and evaporation: development of a laboratory simulation experiment. *Hydrol Process* 13:597–609. [https://doi.org/10.1002/\(SICI\)1099-1085\(199903\)13:4%3c597::AID-HYP756%3e3.0.CO;2-Q](https://doi.org/10.1002/(SICI)1099-1085(199903)13:4%3c597::AID-HYP756%3e3.0.CO;2-Q)
- ASTM Standard D 422-63 (2007) Standard test method for particle-size analysis of soils. ASTM International, West Conshohocken, PA
- ASTM Standard D 4318 (2010) Standard test methods for liquid limit, plastic limit, and plasticity index of soils. ASTM International, West Conshohocken, PA
- ASTM Standard D 854 (2014) Standard test methods for specific gravity of soil solids by water pycnometer. ASTM International, West Conshohocken, PA
- ASTM Standard D 2487 (2017) Standard practice for classification of soils for engineering purposes (unified soil classification system). ASTM International, West Conshohocken, PA
- ASTM Standard D 2216 (2019) Standard test methods for laboratory determination of water (moisture) content of soil and rock by mass. ASTM International, West Conshohocken, PA
- ASTM Standard D 7263 (2021) Standard test methods for laboratory determination of density (unit weight) of soil specimens. ASTM International, West Conshohocken, PA
- Bell B, Hersbach H, Simmons A et al (2021) The ERA5 global reanalysis: preliminary extension to 1950. *Q J R Meteorol Soc* 147:4186–4227. <https://doi.org/10.1002/qj.4174>
- Brater FE, Sherrill JD (1975) Rainfall-runoff relations on urban and rural areas. *Environmental Protection Technology Series* 1–98

- Collins KA, Hunt WF, Hathaway JM (2008) Hydrologic comparison of four types of permeable pavement and standard asphalt in Eastern North Carolina. *J Hydrol Eng* 13:1146–1157. <https://doi.org/10.1061/ASCE1084-0699200813:121146>
- Darama Y (1985) Incorporation a stochastic infiltration capacity into a unit hydrograph method for flood prediction. Michigan State University, M.Sc.
- Darama Y, Yılmaz K, Melek AB (2021) Land degradation by erosion occurred after irrigation development in the Harran plain Southeastern Turkey. *Environ Earth Sci*. <https://doi.org/10.1007/s12665-021-09372-5>
- Darama Y (2000) Prediction of flood frequencies by stochastic-deterministic hydrological model. In: International symposium on river flood defense, kassel reports of hydraulic engineering. Kassel
- Demir A, DİNÇER AE (2023) Efficient disaster waste management: identifying suitable temporary sites using an emission-aware approach after the Kahramanmaraş earthquakes. *Int J Environ Sci Technol*. <https://doi.org/10.1007/s13762-023-05123-0>
- Demir A, DİNÇER AE, YILMAZ K (2023) A novel method for the site selection of large-scale PV farms by using AHP and GIS: a case study in İzmir, Türkiye. *Sol Energy* 259:235–245. <https://doi.org/10.1016/j.solener.2023.05.031>
- DİNÇER AE, DEMİR A, YILMAZ K (2023) Enhancing wind turbine site selection through a novel wake penalty criterion. *Energy* 283:129096. <https://doi.org/10.1016/j.energy.2023.129096>
- DİNÇER AE, DEMİR A, YILMAZ K (2024) Multi-objective turbine allocation on a wind farm site. *Appl Energy* 355:122346. <https://doi.org/10.1016/j.apenergy.2023.122346>
- Döll P, Trautmann T, Gerten D et al (2018) Risks for the global freshwater system at 15 °c and 2 °c global warming. *Environ Res Lett*. <https://doi.org/10.1088/1748-9326/aab792>
- Du J, Cheng L, Zhang Q et al (2019) Different flooding behaviors due to varied urbanization levels within river basin: a case study from the Xiang River Basin, China. *Int J Disaster Risk Sci* 10:89–102. <https://doi.org/10.1007/s13753-018-0195-4>
- EEA (2020) Urban adaptation in Europe: how cities and towns respond to climate change. Luxembourg. <https://doi.org/10.2800/324620>
- Ercolani G, Chiaradia EA, Gandolfi C et al (2018) Evaluating performances of green roofs for stormwater runoff mitigation in a high flood risk urban catchment. *J Hydrol (amst)* 566:830–845. <https://doi.org/10.1016/j.jhydrol.2018.09.050>
- Feldman AD (2000) HEC-HMS Technical Reference Manual. Washington DC
- Ginige K, Mendis K, Thayaparan M (2022) An assessment of structural measures for risk reduction of hydrometeorological disasters in Sri Lanka. *Progress Disaster Sci*. <https://doi.org/10.1016/j.pdisas.2022.100232>
- Hersbach H, Bell B, Berrisford P et al (2020) The ERA5 global reanalysis. *Q J R Meteorol Soc* 146:1999–2049. <https://doi.org/10.1002/qj.3803>
- Huang Y, Tian Z, Ke Q, et al (2020) Nature-based solutions for urban pluvial flood risk management. *Wiley Interdisciplinary Reviews: Water* 7
- IPCC (2022) Global Warming of 1.5°C. Cambridge University Press, Cambridge
- Kreibich H, Bubeck P, Van Vliet M, De Moel H (2015) A review of damage-reducing measures to manage fluvial flood risks in a changing climate. *Mitig Adapt Strateg Glob Chang* 20:967–989. <https://doi.org/10.1007/s11027-014-9629-5>
- Kreibich H, Di Baldassarre G, Vorogushyn S et al (2017) Adaptation to flood risk: results of international paired flood event studies. *Earths Future* 5:953–965. <https://doi.org/10.1002/2017EF000606>
- Liu W, Feng Q, Chen W, Wei W (2020) Assessing the runoff retention of extensive green roofs using runoff coefficients and curve numbers and the impacts of substrate moisture. *Hydrol Res* 51:635–647. <https://doi.org/10.2166/NH.2020.167>
- MGM (2023) Meteoroloji Genel Müdürlüğü-Resmi İstatistikler. <https://www.mgm.gov.tr/veridegerlendirme/il-ve-ilceler-istatistik.aspx>. Accessed 28 Sep 2023
- Nations U, of Economic D, Affairs S, Division P (2018) World Urbanization Prospects The 2018 Revision
- Nigussie TA, Altunkaynak A (2019) Modeling the effect of urbanization on flood risk in Ayamama Watershed, Istanbul, Turkey, using the MIKE 21 FM model. *Nat Hazards* 99:1031–1047. <https://doi.org/10.1007/s11069-019-03794-y>
- Nsangou D, Kpoumié A, Mfonka Z et al (2022) Urban flood susceptibility modelling using AHP and GIS approach: case of the Mfoundi watershed at Yaoundé in the South-Cameroon plateau. *Sci Afr*. <https://doi.org/10.1016/j.sciaf.2021.e01043>
- Papaoiannou G, Efstratiadis A, Vasiliades L et al (2018) An operational method for Flood Directive implementation in ungauged urban areas. *Hydrology*. <https://doi.org/10.3390/hydrology5020024>

- Pathirana A, Denekeew HB, Veerbeek W et al (2014) Impact of urban growth-driven landuse change on microclimate and extreme precipitation - A sensitivity study. *Atmos Res* 138:59–72. <https://doi.org/10.1016/j.atmosres.2013.10.005>
- Prosdociimi I, Kjeldsen TR, Miller JD (2015) Detection and attribution of urbanization effect on flood extremes using nonstationary flood-frequency models. *Water Resour Res* 51:4244–4262. <https://doi.org/10.1002/2015WR017065>
- Ren GY, Zhou YQ, Chu ZY et al (2008) Urbanization effects on observed surface air temperature trends in north China. *J Clim* 21:1333–1348. <https://doi.org/10.1175/2007JCLI1348.1>
- Schwartz SS (2010) Effective curve number and hydrologic design of pervious concrete storm-water systems. *J Hydrol Eng* 15:465–474. <https://doi.org/10.1061/ASCEHE.1943-5584.0000140>
- Shao M, Zhao G, Kao SC et al (2020) Quantifying the effects of urbanization on floods in a changing environment to promote water security — A case study of two adjacent basins in Texas. *J Hydrol (amst)*. <https://doi.org/10.1016/j.jhydrol.2020.125154>
- Sims AW, Robinson CE, Smart CC et al (2016) Retention performance of green roofs in three different climate regions. *J Hydrol (amst)* 542:115–124. <https://doi.org/10.1016/j.jhydrol.2016.08.055>
- Skougaard Kaspersen P, Høegh Ravn N, Arnbjerg-Nielsen K, et al (2015) Influence of urban land cover changes and climate change for the exposure of European cities to flooding during high-intensity precipitation. In: IAHS-AISH Proceedings and Reports. Copernicus GmbH, pp 21–27
- Slater LJ, Villarini G (2016) Recent trends in U.S. flood risk. *Geophys Res Lett* 43:12428–12436. <https://doi.org/10.1002/2016GL071199>
- Slater L, Villarini G, Archfield S et al (2021) Global changes in 20-Year, 50-Year, and 100-Year river floods. *Geophys Res Lett*. <https://doi.org/10.1029/2020GL091824>
- Slinger JH, Cunningham SC, Kothuis BLM (2023) A co-design method for including stakeholder perspectives in nature-based flood risk management. *Nat Hazards*. <https://doi.org/10.1007/s11069-023-06139-y>
- Speak AF, Rothwell JJ, Lindley SJ, Smith CL (2013) Rainwater runoff retention on an aged intensive green roof. *Sci Total Environ* 461–462:28–38. <https://doi.org/10.1016/j.scitotenv.2013.04.085>
- Thives LP, Ghisi E, Brecht DG, Pires DM (2018) Filtering capability of porous asphalt pavements. *Water (switzerland)*. <https://doi.org/10.3390/w10020206>
- Vojinovic Z, Alves A, Gómez JP et al (2021) Effectiveness of small- and large-scale Nature-Based Solutions for flood mitigation: The case of Ayutthaya. *Science of the Total Environment, Thailand*. <https://doi.org/10.1016/j.scitotenv.2021.147725>
- Wang L, Hou H, Li Y et al (2023) Investigating relationships between landscape patterns and surface runoff from a spatial distribution and intensity perspective. *J Environ Manage*. <https://doi.org/10.1016/j.jenvman.2022.116631>
- Waseem M, Ahmad S, Ahmad I et al (2023) Urban flood risk assessment using AHP and geospatial techniques in swat Pakistan. *SN Appl Sci*. <https://doi.org/10.1007/s42452-023-05445-1>
- WMO (World Meteorological Organization) (2012) Integrated Flood Management Tools Series - Flood Proofing. APFM Technical Document No. 15, Flood Management Tool Series. Geneva, Switzerland. [https://www.floodmanagement.info/publications/tools/APFM\\_Tool\\_15.pdf](https://www.floodmanagement.info/publications/tools/APFM_Tool_15.pdf)
- Yang L, Smith JA, Wright DB et al (2013) Urbanization and climate change: An examination of nonstationarities in urban flooding. *J Hydrometeorol* 14:1791–1809. <https://doi.org/10.1175/JHM-D-12-095.1>
- Yılmaz K, Dinçer AE, Kalpakçı V, Öztürk Ş (2022) Debris flow modelling and hazard assessment for a glacier area: a case study in Barsem Tajikistan. *Nat Hazards*. <https://doi.org/10.1007/s11069-022-05654-8>
- Yılmaz K, Darama Y, Oruc Y, Melek AB (2023a) Assessment of flood hazards due to overtopping and piping in Dalaman Akköprü Dam, employing both shallow water flow and diffusive wave equations. *Nat Hazards* 117:979–1003. <https://doi.org/10.1007/s11069-023-05891-5>
- Yılmaz K, Dinçer AE, Ayhan EN (2023b) Exploring flood and erosion risk indices for optimal solar PV site selection and assessing the influence of topographic resolution. *Renew Energy* 216:119056. <https://doi.org/10.1016/j.renene.2023.119056>
- Zhai R, Tao F, Lall U et al (2020) Larger drought and flood hazards and adverse impacts on population and economic productivity under 2.0 than 1.5°C warming. *Earths Future*. <https://doi.org/10.1029/2019E001398>
- Zhang Z, Szota C, Fletcher TD et al (2018) Influence of plant composition and water use strategies on green roof stormwater retention. *Sci Total Environ* 625:775–781. <https://doi.org/10.1016/j.scitotenv.2017.12.231>
- Zhang Z, Szota C, Fletcher TD et al (2019) Green roof storage capacity can be more important than evapotranspiration for retention performance. *J Environ Manage* 232:404–412. <https://doi.org/10.1016/j.jenvman.2018.11.070>

**Publisher's Note** Springer Nature remains neutral with regard to jurisdictional claims in published maps and institutional affiliations.

GCPRIS